Construction and Building Materials 266 (2021) 120969

Contents lists available at ScienceDirect

Construction and Building Materials

journal homepage: www.elsevier.com/locate/conbuildmat

Optimization for the preparation of composite geopolymer using response surface methodology and its application in lead-zinc tailings solidification

Shujie Zhao [a,b,1], Ming Xia [a,b,1], Lin Yu [b,1], Xiao Huang [a,b,*], Binquan Jiao [a,b,*], Dongwei Li [a,b,*]

[a] State Key Laboratory for Coal Mine Disaster Dynamics and Control, Chongqing University, Chongqing 400044, PR China
[b] School of Resources and Safety Engineering, Chongqing University, Chongqing, 400044, China

HIGHLIGHTS

- The feasibility study of geopolymer with high strength based on uncalcined coal gangue and blast furnace slag was conducted.
- Response surface method was adopted for the optimization of preparation of composite geopolymer.
- The effective solidification of heavy metals in lead-zinc tailing were achieved.
- Solidified bodies have potential for application of construction purpose.

ARTICLE INFO

Article history:
Received 23 June 2020
Received in revised form 27 August 2020
Accepted 12 September 2020

Keywords:
Lead-zinc tailing
Coal gangue
Solidification
Composite geopolymer
Heavy metal
Response surface methodology

ABSTRACT

The improper disposal of solid wastes could bring great pressures and threats to ecosystem. These detrimental impacts could be reduced or eliminated through solidification/stabilisation technology based on geopolymer. In this paper, composite based geopolymer prepared from coal gangue and blast furnace slag was used for the solidification of heavy metals in lead–zinc tailing (LZT). The impact of various factors on compressive strength development in composite geopolymer was evaluated through response surface experiment. Additionally, the sample with maximum strength (91.13 MPa) was chosen to solidify LZT. The results showed that strength of solidified bodies with addition of 70% LZT fell to 21.68 MPa. Based on leaching tests, these samples could potentially be used for construct applications, since leaching concentrations were far below the standard limits. Heavy metals in LZT were effectively solidified via physical and chemical ways, which was evidenced by chemical speciation analysis, mercury intrusion porosimetry, X-ray diffraction and scanning electron microscope with energy dispersive spectrometry analyses.

© 2020 Elsevier Ltd. All rights reserved.

1. Introduction

In 2017, the proportion of raw coal in China's total energy production was more than 69% [1]. The development of coal mining industry has brought great pressure on the environment. Coal gangue (CG) is a waste generated in the process of coal mining and coal washing. The total output in China is around 4.5–5.0 billion tons [2]. Long-term stockpiling and improper disposal of CG may not only occupy farmlands but also threaten both the surrounding environment and human health. With the growing recognition of environmental protection, the reutilization of CG has been concerned about. The aluminosilicate components in CG could be used for preparation of geopolymer. This enables large amounts of industrial solid wastes (e.g. CG) to be recycled and reused.

Geopolymer is a new inorganic material with analogous cementitious properties to Ordinary Portland Cement (OPC). Recently, it has received increasing attention owing to its advantages, such as low emission of CO_2, excellent mechanical properties, low permeability, and high resistance to common hostile environments in the natural (e.g., acidic, seawater and high-temperature conditions) [3–7]. Geopolymer is synthesised from a series of the dissolution-recombination-gelation-hardening-crystallization reactions between raw materials and alkaline solutions [8]. The source materials include industrial by-products/wastes and

* Corresponding authors at: State Key Laboratory for Coal Mine Disaster Dynamics and Control, Chongqing University, Chongqing 400044, PR China.
E-mail addresses: shawwong@126.com (X. Huang), j.binquan@cqu.edu.cn (B. Jiao), litonwei@cqu.edu.cn (D. Li).
[1] These authors contributed equally to the work.

https://doi.org/10.1016/j.conbuildmat.2020.120969
0950-0618/© 2020 Elsevier Ltd. All rights reserved.

natural minerals containing aluminosilicates. According to the chemical composition, these raw materials can be categorised into two types, i.e. low calcium and high calcium. The reaction product of low calcium materials including metakaolin, fly ash and CG is N-A-S-H type gel. In terms of high calcium materials e.g. blast furnace slag (BFS), C-A-S-H gel is formed after alkaline activation. At the same time, calcium-based hydration products i.e. C-S-H gel are produced in the presence of water. In addition, C-S-H gel will coexist with (N, C)-A-S-H gels when two kinds of raw materials are used simultaneously [9–13]. As for geopolymer, the kind and quantity of the formed gels play a big part in obtaining its high mechanical performance and durability [14,15].

The performance of geopolymer prepared with raw CG is poor due to its stable crystal structures such as kaolinite and quartz leading to the low cementitious activity. To achieve better properties of geopolymer, the reactivity of CG is commonly promoted by thermal activation (i.e. calcination) [16–18]. However, the heating process consumes considerable energy likewise OPC. To conserve the heat energy, several scientists had achieved the preparation of geopolymer using raw kaolin without calcination [19–21]. On the other hand, the coordinative usage of several raw materials in the preparation of geopolymer recently has drawn public attention. BFS is a by-product of iron-making industry. When the high calcium material i.e. BFS is introduced into the low calcium geopolymer system, CaO could participate in the reaction and generate C-S-H/C-A-S-H gels as well as N-A-S-H gel, which improve the strength development of geopolymer matrix. Besides, using these two abundant waste materials i.e. CG and BFS to prepare geopolymer is of environmental benefit.

Heavy metal pollution caused in the exploitation and utilization of nonferrous mineral resources is another real environmental issue. With the large-scale exploitation of lead-zinc mine, a massive amount of residues i.e. lead–zinc tailings (LZT) containing Pb^{2+}, Zn^{2+}, Cd^{2+} and other heavy metals is generated. These heavy metals might leach out into groundwater and soil, and then endangers human health over time. Solidification/stabilisation technology is considered as the efficient approach with regard to the treatment of waste containing heavy metals [22–24]. The application of geopolymer as solidifying agent has raised more attention due to its high immobilization efficiency, low cost and green environmental protection. Muhammad et al. had found that through chemical bonding and physical encapsulation, composite geopolymer effectively immobilized Pb^{2+}, Cr^{3+} and Cd^{2+} within reasonable range [25]. Ye et al. had productively solidified municipal solid waste incineration fly ash containing Pb^{2+}, Cu^{2+}, Zn^{2+} and Cr^{3+} with geopolymer [26]. Chen et al. had achieved the co-disposal of shell coal gasification fly ash and steel slag through geopolymer technology, in which the leaching of heavy metals was below the limit [27]. The solidification mechanism of Pb^{2+}, Cd^{2+} and Cu^{2+} in metakaolin-based geopolymer was researched by Ei-Eswed et al. [28]. They revealed that these toxic metal cations were effectively solidified in geopolymer through bonding with nonbridging oxygen ions such as Si-O^{-} and Al-O^{-}, or forming compounds i.e. carbonates.

Generally speaking, mechanical properties and leaching concentration are the measures of solidification efficiency of heavy metals in geopolymer. However, compressive strength is inversely proportional to leaching concentration [29]. In addition, the compressive strength of geopolymer matrix is susceptible to many factors including source material, curing temperature, liquid/solid ratio, alkali activator ratio, as well as nature and concentration of wastes [30–32]. Determination of optimal synthesis parameters is the key to developing more products with practicability. Thus, a robust tool named response surface methodology (RSM) was employed for designing experimental plans regarding the preparation of geopolymer and optimizing the results. RSM is a product of combining mathematics with statistical methods. Compared with single-factor and orthogonal design methods, experimental designing with RSM has the following advantages: a) fewer times of experiments b) establishment of a statistical model of factors and response c) evaluation of interrelation between relevant parameters d) optimization of the outcomes within reasonable region.

Preparation of CG-BFS based composite geopolymer (CBG) and solidification of LZT were conducted in this paper. One objective of this research was to explore the interrelation of variables (i.e. waterglass module, alkaline content and curing temperature) and compressive strength by using RSM, as well as to optimize synthesis process conditions to obtain higher strength of the matrix. Additionally, solidification efficiency of LZT in the composite geopolymer was researched. The MIP, XRD, SEM-EDS and speciation analyses were used to further analyse and explore properties and solidification mechanism of composite geopolymer.

2. Materials and methods

2.1. Materials

The CG used in this work was obtained from a colliery in Shanxi, China, and the BFS was brought from a steelworks located in Chongqing, China. The lead–zinc tailing (LZT) was taken from a metallic mine situated in Yunnan, China. Analytical grade sodium hydroxide, industrial grade water glass (modulus 3.0) and deionized water were used to synthesize the alkali activator throughout the experiment. Table 1 presents the chemical composition of raw materials. Additionally, the total contents of toxic components with environmental risk in LZT are as follows Zn 35979 mg/kg, Pb 1216 mg/kg and Cd 351 mg/kg, respectively.

Fig. 1 depicts the XRD patterns of raw materials i.e. BFS, CG and LZT. The XRD spectrum of BFS mainly was amorphous and accompanied by a weak peak of gehlenite, ($2CaO{\cdot}Al2O_3{\cdot}SiO_2$, PDF# 35-0755), while in that of CG sharp peaks of kaolinite ($Al_2Si_2O_5(OH)_4$, PDF# 75-1593) and quartz (SiO_2, PDF# 85-0695) were identified. Besides, sharp diffraction peaks representing quartz (SiO_2, PDF# 85-0865), calcium carbonate ($CaCO_3$, PDF# 70-0095) and ilvaite ($HCaFe_2FeO_2(Si_2O_7)$, PDF# 75-1734) were observed in LZT, in which quartz peak at 2θ of about 27° was extremely sharp.

2.2. Methods

2.2.1. Preparation of composite based geopolymer

CG was mixed with BFS at a ratio of 1:1 and then the mixture was stirred into the activator solution. The ratio of liquid to solid was 0.27. Afterwards, the prepared paste was poured into a cube mould with 20 mm per edge, vibrated 5 min to reduce bubbles and cured at the given temperature. After 24 h, the specimens were

Table 1
Chemical compositions of CG, BFS and LZT (wt%).

	SiO_2	Al_2O_3	Fe_2O_3	TiO_2	K_2O	CaO	MgO	SO_3	Na_2O
CG	59.52	36.57	1.24	1.14	0.75	0.26	0.18	0.16	N.D.
BFS	35.62	14.93	0.60	1.28	0.39	36.31	7.50	2.29	0.22
LZT	62.09	4.34	2.72	0.20	0.54	20.44	0.56	3.62	N.D.

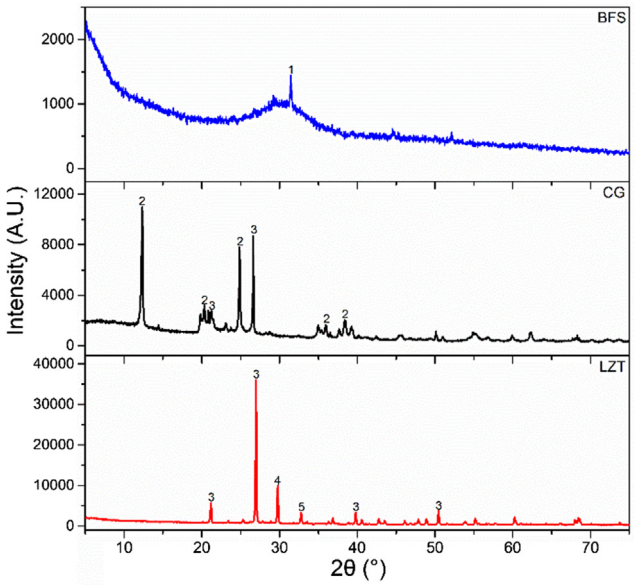

Fig. 1. XRD patterns of raw materials i.e. BFS, CG and LZT, 1-Gehlenite, 2-Kaolinite, 3-Quartz, 4- Calcium carbonate and 5- Ilvaite.

demoulded and cured at room temperature until 28 d for testing. The detailed experimental scheme was devised using the central composite design that is a commonly used method in RSM. Table 2 listed the corresponding codes and levels of each factor (i.e. alkaline content, waterglass module and curing temperature). Twenty-three mix proportions of composite geopolymer paste are given in Table 3. There are nine randomised duplications of the central point to improve experimental accuracy and prevent possible errors. Additionally, the relationships between these independent parameters and output response i.e. compressive strength were investigated and optimum variables combination for achieving maximum strength of the matrix was determined. The concerned calculations were made using Microsoft Excel 2016.

2.2.2. Solidification/stabilisation of LZT

The CG-BFS based composite geopolymer obtained under optimal conditions (Section 2.2.1) was used as curing agent for solidifying LZT. Various proportions of LZT (30, 40, 50, 60 and 70 wt%) as substitution to CG-BFS mixture were conducted as aim for preparing solidified bodies. The other experiment conditions remained constant.

2.2.3. Compressive strength tests

The compressive strength was measured by AGN-250 universal testing machine (Shimadzu, Japan). To reduce errors, the mean value of measurement results of three repeated samples was adopted as the final strength for specimen.

2.2.4. Leaching tests

Toxicity characteristic leaching procedure (TCLP) [33] established by United States Environmental Protection Administration

Table 2
Boundaries of factors in RSM.

Factors	Coded levels				
	−1.682	−1	0	1	1.682
A: Waterglass module	0.2	0.4	0.7	1	1.2
B: Alkali content (wt%)	2.5	5.54	10	14.46	17.5
C: Curing temperature (℃)	30	38	50	62	70

Table 3
Experimental scheme and the corresponding results.

Test number	A	B	C	Compressive strength (MPa)
1	1	1	−1	85.62
2	−1.682	0	0	28.72
3	0	−1.682	0	32.28
4	0	0	0	69.97
5	−1	1	1	39.08
6	0	0	0	69.14
7	0	0	0	66.77
8	1.682	0	0	59.36
9	0	0	−1.682	73.77
10	1	−1	1	45.11
11	1	−1	−1	61.28
12	0	1.682	0	52.10
13	−1	−1	1	36.89
14	0	0	0	69.51
15	0	0	1.682	46.83
16	−1	1	−1	52.29
17	1	1	1	37.43
18	0	0	0	69.77
19	0	0	0	64.64
20	0	0	0	63.15
21	−1	−1	−1	33.85
22	0	0	0	67.31
23	0	0	0	75.36

was utilized to evaluate the leaching toxicity of heavy metals in raw LZT and solidified bodies containing LZT. To prepare the extraction solution, the acetic acid (CH_3CH_2OOH) were added in deionized water (to adjust the pH value at 2.88 ± 0.05). The extraction solution with crushed sample (<9.5 mm) was shaken for 18 h at 30 rpm with liquid to solid ratio of 20. Then the leaching solution was filtered with 0.45 μm microporous filter and the concentrations of heavy metals (Zn^{2+}, Pb^{2+} and Cd^{2+}) were measured through atomic absorption spectrometer in accordance with GB 5085.3–2007 [34]. The immobilization ratio of solidification products were assessed according to formula (1).

$$\text{Immobilization rate} = 1 - \frac{\text{Mass of each toxic heavy metal in the leaching solution}}{\text{Total mass of each toxic heavy metal in the initial solid}} \quad (1)$$

2.2.5. Chemical speciation analyses of heavy metals

Chemical speciation analyses of heavy metals were measured based on Tessier's sequential extraction method [35] and there are five basic steps in the whole process (Table 4). 1 g sample was used at the beginning of the test. At the end of every step, upper liquid was obtained through centrifugation at 4000 rpm for 20 min to determine metal concentrations in corresponding fraction. Additionally, the remnants were washed with deionized water and then continued to be used for the next step. Generally

Table 4
Sequential extraction scheme.

Step	Fraction	Reagent and concentration
1	Exchangeable	1 M $MgCl_2$ (8 mL), pH 7 shaken 1 h at room temperature
2	Acido-soluble	1 M HOAc (8 mL) shaken 8 h at room temperature
3	Reducible	0.04 M $NH_2OH{\cdot}HCl$ in 25% (v/v) HOAc (20 mL), shaken 4 h at 96 °C
4	Oxidizable	30% (v/v) H_2O_2 (5 mL), pH 2 shaken 2 h at 85 °C; then H_2O_2 (3 mL), pH 2 shaken 3 h at 85 °C; after cooling, 3.2 M NH4OAc in 20% (v/v) HNO_3 (5 mL), diluted to 20 mL, shaken 0.5 h
5	Residual	HF–HClO4 digestion

speaking, every metal could be divided into five forms, including exchangeable, carbonates, Fe-Mn oxides, organic matters/sulphides and residual. Exchangeable and carbonates fractions are available under natural conditions, Fe-Mn oxides and organic matters/sulphides are potentially available in reducing environments, and residual fraction is unable to leach.

2.2.6. Characterization identification

The chemical composition of raw materials i.e. CG, BFS and LZT was determined by using X-ray fluorescence spectrometry (XRF, Shimadzu, Japan). The determinations of mineralogical compositions, pore structures and morphological characteristics of samples were carried out with the help of MIP, XRD, and SEM-EDS. MIP was conducted by using a mercury intrusion meter with maximum pressure of 33,000 Psi (PoreMaster-33, American). XRD was performed using X'Pert PRO (PANalytical B.V., Netherlands) with CuK_{α} radiation in the 2θ range of 5 to 75°. SEM-EDS was performed using the Filament SEM instrument (VEGA3 TESCAN, Czech Republic) at an accelerated voltage of 15 kV.

3. Results and discussion

3.1. Optimization of composite geopolymer mix proportion based on RSM

Table 3 summarized the compressive strength values of composite geopolymer specimens prepared based on the experimental design. These experimental data were analysed by using regression analytic method. It was found that the response i.e. compressive strength followed a quadratic model. The following regression equation linking the response to independent variables was constructed.

$$\begin{aligned} \textit{Compressive strength} = & -186.594 + 255.682\,A \\ & + 15.868\,B + 3.544\,C \\ & - 1.899\,AC - 0.114\,BC \\ & - 94.013\,A^2 - 0.451\,B^2 \\ & - 0.018\,C^2 \end{aligned} \quad (2)$$

3.1.1. Verification of model

The analysis of variance (ANOVA) was used to verify the significance of the established model and the correctness of description regarding the data relationship [36]. In present study, the confidence level maintained 95%. The lower p-value is, statistically, the more significant of corresponding term. The p-value for the compressive strength model was less than 0.0001 (Table 5), indicating the model was of significance. However, it is not necessarily true that the explanation as to the changes in data is proper. The following terms are requisite for correct analyses of data, including lack of fit analysis, R^2 values and so on [37,38]. The lack of fit test also supported that the established model was acceptable (Table 5). Besides, high adj-R^2 value (0.9582) indicated that the built model could explain 95.82% of the change in compressive strength of composite geopolymer. The value of multiple R was 0.9866, which implied that the fitting degree was good and experimental error is small. Additionally, Fig. 2 presents the experimental and model-predicted data could be fitted into a line. The R^2 of 0.9981 indicated a good agreement between estimated and actual data [39], which corroborated the validation of the built model again.

3.1.2. Impact of variables over the strength

ANOVA also could point the significant terms and describe their relative contribution to the response i.e. compressive strength (Table 6 and Fig. 3). The bar graph clearly illustrates that among the first order terms, the contribution ratio of curing temperature and waterglass module to compressive strength was roughly equal (about 18.50%), whereas that of alkali content was minimal, accounting for 6.54%. However, the quadratic term of alkali content had a very remarkable influence on strength. In addition, the interaction of temperature with waterglass module had comparatively greater impact on strength comparing to its interaction with alkali content.

The compressive strength changed as a function of temperature and waterglass module at an alkali content of 10% presented in

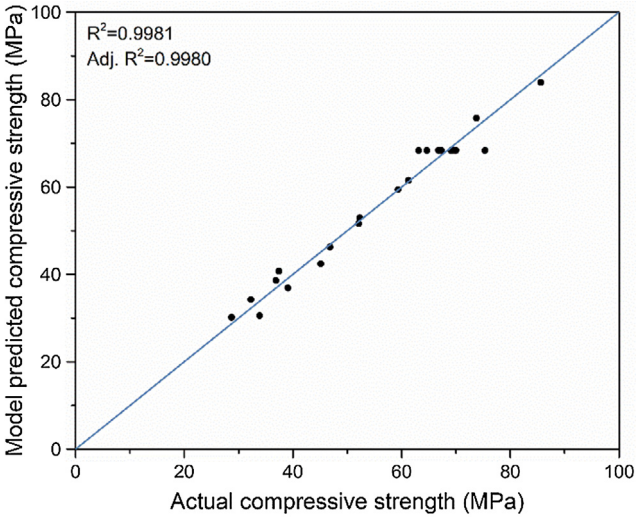

Fig. 2. Predicted vs actual experimental data.

Table 6
Significant test of the regression coefficients.

Terms	Coefficients	t stat.	p-value
Intercept	−186.594	−8.292	<0.0001
A	255.682	12.093	<0.0001
B	15.868	11.383	<0.0001
C	3.544	5.287	0.0001
AA	−94.013	−10.076	<0.0001
BB	−0.451	−10.834	<0.0001
CC	−0.018	−3.100	0.0078
AC	−1.899	−5.806	<0.0001
BC	−0.114	−5.172	0.0001

Table 5
ANOVA of the compressive strength model.

	Quadratic sum	Freedom	Mean square	F value	P value
Model	5583.203	8	697.900	64.086	<0.0001
Residual error	152.461	14	10.890		
Lack of fit	52.353	6	8.725	0.697	
Pure error	100.108	8	12.514		
Sum	5735.664	22			

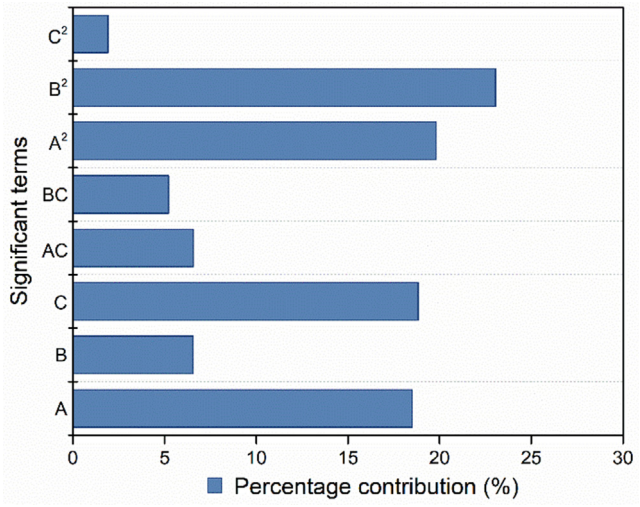

Fig. 3. Percentage contribution of significant model terms on compressive strength.

Fig. 4(a). The waterglass module in reasonable range had a notable positive impact on compressive strength. That happened because the greater waterglass module signified the alkaline solution contained higher concentration of $[SiO_4]^{4-}$, thus favouring the reaction between dissolved Ca^{2+} from BFS and $[SiO_4]^{4-}$ in the alkaline solution. The formed C-S-H gel could fill the pore, improving the compactness of paste. Additionally, the high-viscosity Na_2SiO_3 also could promote the formations of geopolymer gels and dense microstructure, thus leading to good mechanical properties of geopolymer [40]. These results were in accordance with Çelikten et al. [14]. The increase in compressive strength with waterglass module became smaller as curing temperature increased. For instance, as waterglass module increased from 0.4 to 1.0, the strength rose from 30 MPa to 80 MPa at 30 °C and from 20 MPa to 50 MPa at 70 °C. As some authors reported, low curing temperature is conductive to the hydration reaction of BFS, while CG possessed low geopolymerization reactivity in this condition [41–43]. Therefore, it might be considered that the reaction at 30 °C may be dominated by the hydration reaction of BFS, while the reaction at 70 °C could be due to the interaction between CG and BFS. Furthermore, the water evaporation at elevated temperature might cause the formation of pores as well as cracks, and inhibit the polycondensation reaction [3]. Hence, strength decreased with increasing temperature.

As shown in Fig. 4(b), the variation trend of compressive strength with alkali content and cuing temperature was alike to that of strength with waterglass module and temperature. The compressive strength increased along with alkali content and then decreased gradually after reaching the peak. Compared with SiO_2 and $Al2O_3$, CaO in BFS was easier to dissolve in alkaline solution [44]. The continuous consumption of Ca^{2+} resulting from the formation of hydration products containing Ca^{2+} improved the dissolution rate of BFS. As a result, the higher alkalinity of solution was in favour of the disintegration of CG. Moreover, the formed C-S-H could act as nucleation sites, thus accelerating the dissolution process of raw materials [45]. Thus, the later reaction i.e. rearrangement, gelation and hardening occurred earlier. In other words, raising the alkali content could improve the reaction extent [46]. Additionally, the alkali metal cations could stabilise the structure of geopolymer through charge balancing. Consequently, strength increased. However, an overdose of alkali activator weakened the strength of matrix due to the formation of carbonates. At low alkali content, elevating the curing temperature resulted in slight fluctuations of compressive strength, whereas at higher alkali content the compressive strength decreased markedly with temperature. For example, the change of compressive strength was small when temperature increased from 30 °C to 70 °C at the alkali content of 2.5%, however at 17.5% alkali content the same temperature variation led to a drop from 89 MPa to 24 MPa. Briefly, these changes in compressive strength were the result that waterglass module, alkali content and curing temperature acted together.

3.1.3. Optimization and validation experiments

After building and verifying the model for compressive strength, the optimal experiment conditions maximizing the strength were found out. Note that every factor i.e. waterglass module, alkali content and curing temperature was within a certain range to avoid extrapolation. It was found that the optimum technological conditions are waterglass module 1.06, alkali content 13.81%, and curing temperature 30 °C. The compressive strength could reach 94.41 MPa. Three verification experiments were conducted according to the aforementioned conditions. The average of measured strength was 91.13 MPa with a small deviation

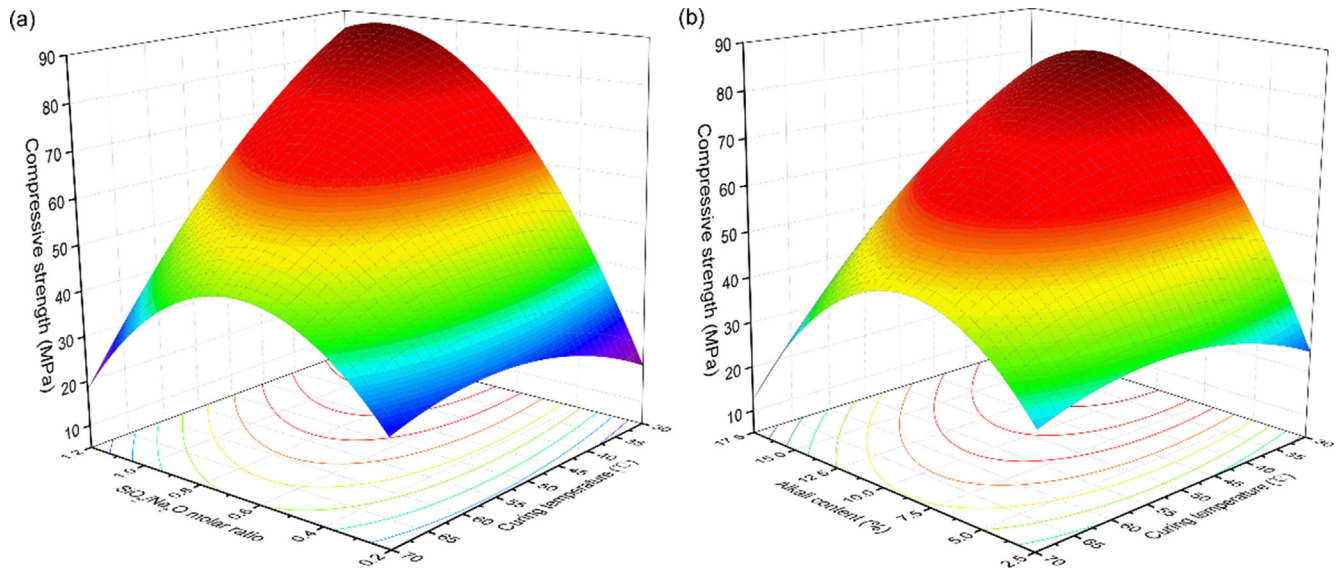

Fig. 4. Response surface curves among input variables and compressive strength.

(4.01%), which indicated the predict precision of the developed model was satisfactory.

3.2. Solidification of LZT

3.2.1. Compressive strength of solidified bodies containing LZT

It is requisite for the solidified bodies to have enough compressive strength against external forces. Fig. 5 presents that the compressive strength of solidified products reduced with introducing of LZT. Due to the low content of active substances in LZT (Section 2.1), adding a high proportion of LZT caused the reduction of active components in the mixture, which might lead to changes in the structure. Specifically, the incorporation of LZT might result in a decrease in the amount of produced gels and the formation of porous structure. Hence, strength decreased, in consistent with previous researches [47,48]. However, the compressive strength of the specimens produced with 70 wt% LZT was still greater than 21 MPa, which provides a possible application for construction purpose. This might be because of the existence of gels i.e. (N, C)-A-S-H and C-S-H. Meanwhile, some heavy metal compounds could be in favour of the development of strength [49]. The low mechanical strength of geopolymer product rich in LZT could be attributable to the ingredient of low reactivity in LZT was less vulnerable to alkali attack, so that there was not a sufficient number of formed gels in the matrix. As a result, the pore structure changed and the geopolymeric structure became weakened or even was destroyed under this condition. Thus, strength dropped off.

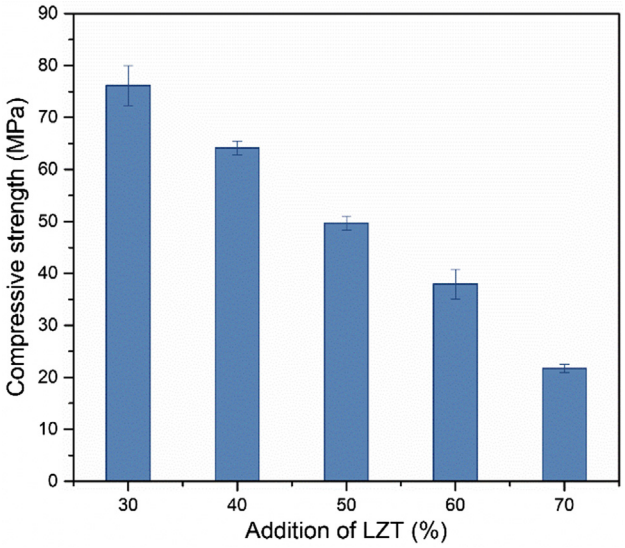

Fig. 5. Compressive strength of solidified bodies containing LZT.

3.2.2. Leaching tests

As mentioned before, the strength of solidified bodies was acceptable. However, the leaching concentrations of heavy metals i.e. Zn^{2+}, Pb^{2+} and Cd^{2+} measured in raw LZT were 540.27, 37.03 and 6.37 mg/L, respectively. And Pb^{2+} and Cd^{2+} exceeded the corresponding limits of TCLP (Pb^{2+}=5 mg/L and Cd^{2+}=1 mg/L). Therefore, it is very necessary to consider the leaching toxicity of heavy metals of solidified products.

Fig. 6 shows that although the leaching concentration of heavy metals increased with increment of LZT content, they were all within the limits. It was evidence that the CG-BFS based cementitious geopolymers could effectively solidify these toxic metals. The immobilization of heavy metals is tightly related to the microstructure and composition of geopolymer matrix [50,51].With the addition of LZT, the concentration of heavy metals in the leaching solution grew owing to the variation of structure. More concretely, the formation of polymerization and hydration products concerned with the physical or chemical encapsulation regarding heavy metals reduced. Notably, the leaching of these toxic metals i.e. Zn^{2+}, Pb^{2+} and Cd^{2+} were within the permissible limits although the concentration increased. By contrast, the leaching concentration of Zn^{2+} was apparently higher than that of Pb^{2+} and Cd^{2+}, which could be ascribed with the higher Zn^{2+} content in raw LZT. Besides, the immobilization rate of each toxic metal of solidified bodies were higher than 97.80%, implying that CG-BFS based geopolymer was very efficient for immobilizing these heavy metals of LZT and transforming hazardous LZT to green environmental materials.

3.2.3. Characterization analysis of solidified bodies

(1) Distribution of heavy metals fractions

The speciation distributions of Zn^{2+}, Pb^{2+} and Cd^{2+} in raw LZT and CBL50 specimen were measured, and the results are presented in Fig. 7. In the raw LZT, Zn^{2+} was dominated by the residue fraction, followed by Fe-Mn oxides fraction, organic matters/sulphides fraction and carbonates fraction, while Pb^{2+} mainly existed in carbonates fraction and Fe-Mn oxides fraction, and for Cd^{2+}, the Fe-Mn oxides fraction dominated. The sequential extraction experiment demonstrated that most of Pb^{2+} in carbonates fraction and Fe-Mn oxides fraction migrated to residual form, leading to a decrease in its leachability. This is in line with the results shown in Fig. 6 and consistent with Lee et al. [52]. Additionally, the proportion of residual fraction for Zn^{2+} was up to 91%. Regarding Cd^{2+}, the proportion of former three forms (i.e. exchangeable, carbonates and

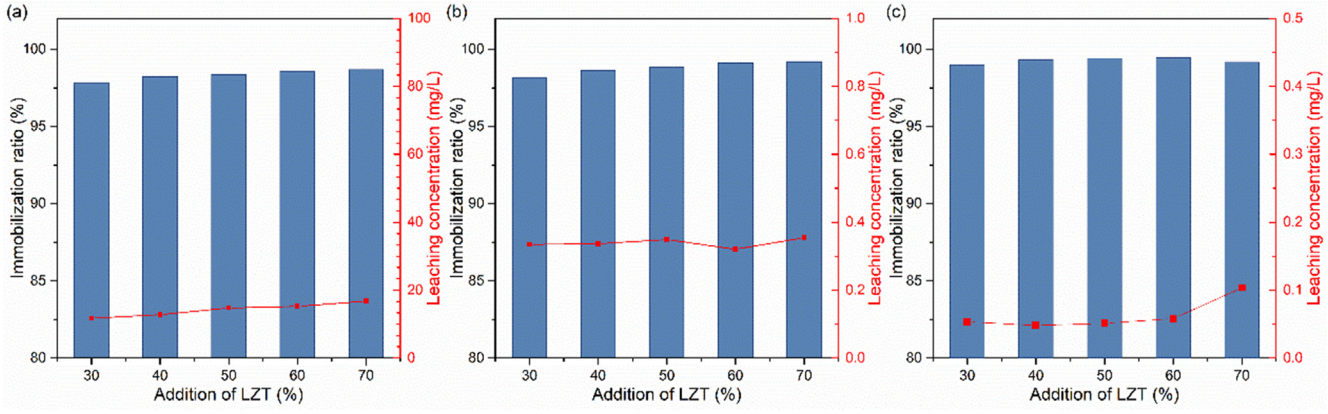

Fig. 6. Immobilization ratio and leaching concentration of (a) Zn^{2+}, (b) Pb^{2+} and (c) Cd^{2+}.

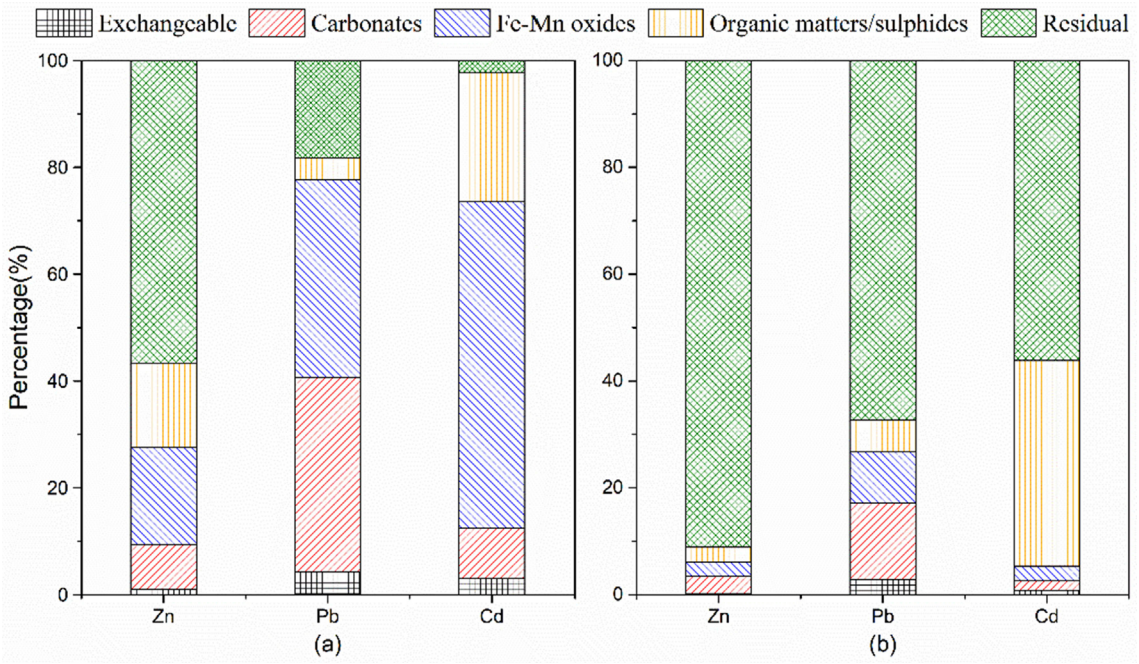

Fig. 7. Chemical speciation distributions of Zn^{2+}, Pb^{2+}, Cd^{2+} in (a) raw LZT, and (b) CBL50.

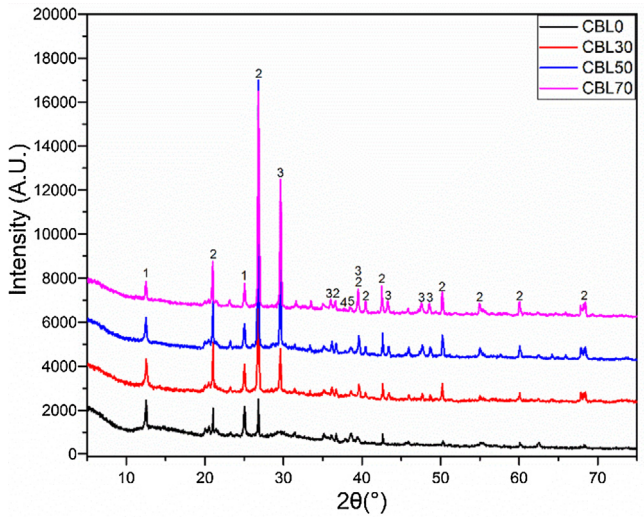

Fig. 8. XRD patterns of solidified bodies containing LZT, 1-Kaolinite, 2-Quartz, 3-Calcium carbonate, 4-Fraipontite-2M1 and 5-Amesite-2H, ferroan.

Fe-Mn oxides forms) declined and that of residual form rose significantly. The transformation and migration results revealed that Zn^{2+}, Pb^{2+} and Cd^{2+} could react chemically with T-O (T = Si, Al) bonds in geopolymer or be captured in structural cavities [53]. Therefore, the CG-BFS based composite geopolymer had an excellent chemical solidification effect to these metals and could reduce the possibility of their exposure to the environment.

(2) Mineralogical compositions analysis

The XRD patterns of solidified products containing LZT show that there mainly were crystalline peaks and dispersion humps (Fig. 8). These Ababneh et al. pointed out that the dispersion hump peak at around 30° which was overlapped with $CaCO_3$ was related to C-S-H [13]. The CSH gel was generated from the hydration reaction of BFS. Specifically, Ca^{2+} dissolved from CaO in BFS could react with $[SiO_4]^{4-}$ from alkaline solution or raw materials, thus forming C-S-H. Additionally, the gel phases such as N-A-S-H and C-(A)-S-H might be generated in the composite geopolymers. There was no clear line between these gels [54]. However, they were hard to detect in XRD images because of their coexistence and overlapping with crystalline peaks [55]. Moreover, it was also noticed that some new phases e.g. fraipontite-2 M1 ($(Zn, Al)_3(Si, Al)_2O_5(OH)_4$,

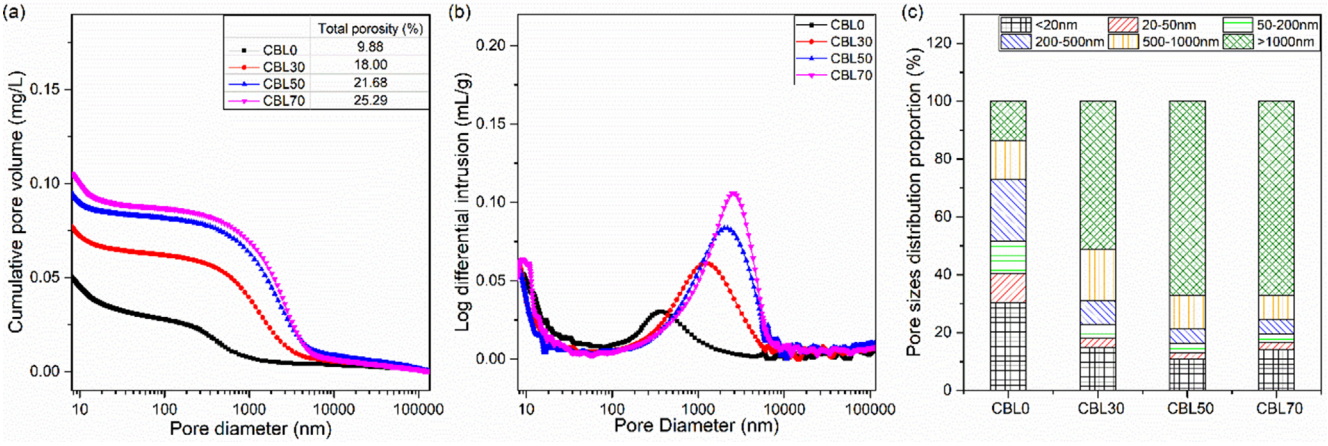

Fig. 9. Pore structures of CBL0, CBL30, CBL50 and CBL70.

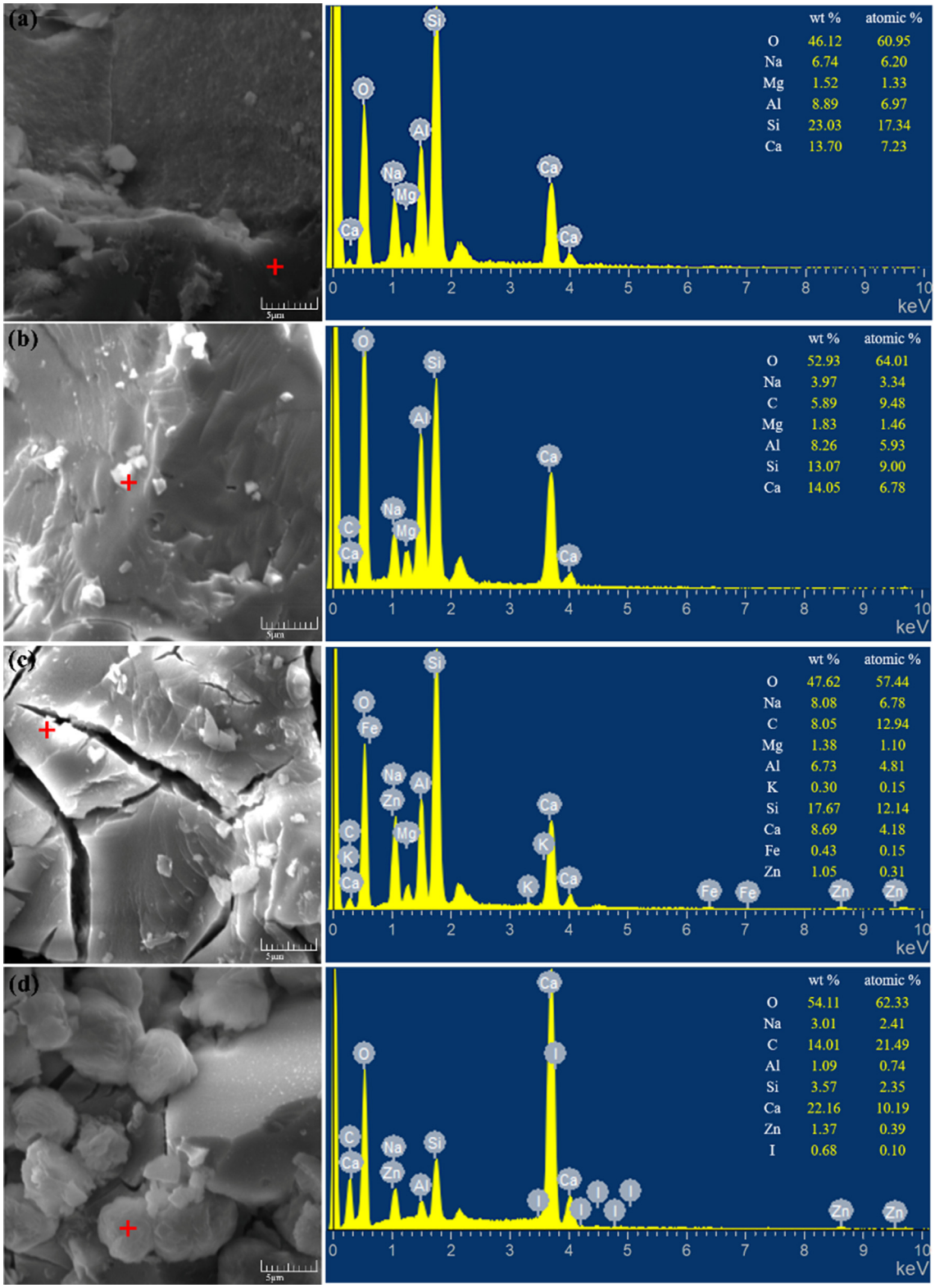

Fig. 10. The SEM images and EDS spectra of (a) CBL 0, (b) CBL 30, (c) CBL 50 and (d) CBL-

PDF# 14–0366) and amesite-2H, ferroan ($(Mg, Fe)_2Al(Si, Al)_2O5(OH)_4$, PDF# 37–0429) appeared. It indicated that structure of raw materials was recombined/rearranged after alkaline activation and toxic metals might be introduced into the geopolymeric structure to be solidified effectively [28,47].

(3) Pore structure analysis

MIP tests were carried out to examine the pore structure of the composite geopoylmer. Under the external pressure, mercury is squeezed into the largest holes of samples first, and finally small holes. Therefore, with decrease in pore size, the cumulative pore volume curve showed an upward trend (Fig. 9(a)). It was clear that the cumulative pore volume of CBL0 was lower than that of solid-

ified bodies containing LZT. Besides, the total porosity of control sample (CBL0) was the minimal at 9.88%. In comparison with the control, the total porosity of CBL30 (18.00%) increased by 82.17%, whereas that of CBL70 (25.29%) grew by 155.97%. This might reveal the possible reason why compressive strength at high LZT content reduced. Generally, the smaller the cumulative pore volume and total porosity are, the more compact is the structure of specimen [56,57]. It could be considered that the structure of samples became weaker with increase in LZT content, leading to a decrease in compressive strength, coherent with other reported results [58].

Log differential curves in Fig. 9(b) show that there are two peaks. Pore sizes of samples were mainly distributed in the range of <20 nm and 100–10000 nm, belonging to meso- and macroscopic pores categories. With the proceeding of geopolymerisation, the newly as-generated hydration products probably blocked voids, which resulted in the formation of two different types of pore systems [59]. The incorporation of LZT reduced the generation of geopolymer phases. Therefore, some changes happened in the pore structure.

To further research the variation of pore size distributions of samples, pore size was subdivided into six parts and proportions of each part to total pore volume was calculated. And the results are presented in Fig. 9(c). There is an obvious tendency. With increasing LZT content in composite geopolymer, the quantity of harmless (<20 nm), less harmful (20–50 nm) and harmful (50–200 nm) pores decreased, and that of more harmful (>200 nm) pores increased. The percentage of harmless pores dropped by more than 50%, from 30.29% in CBL0 specimen to less than 15% in CBL70. Besides, the percentage of less harm and harmful pores showed a marked decrease of over 70%, while that of more harmful pores rose about 66%. It is noteworthy that the percentage of larger than 1000 nm pores in CBL70 was comparatively higher, reaching to 67.12%, and about 5 times as much as that in CBL0. The low reactivity of LZT might cause the existence of great quantity of unreacted LZT residues in the composite geopolymer, which increased the number and size of large voids. This is in line with the observation from SEM. From micro aspect, the surge of number of these large pores or more harmful pores was possibly the primary reason for the decrease of compressive strength of composite geopolymers.

(4) Morphological structure analysis

The EDS spectra displayed that the structure of CBL0 was mainly composed of Si, Al, Na and Ca species after alkaline activation process (Fig. 10(a)). Besides, a high ratio (2.96) of $(M_{Na} + M_K + 2\text{-}M_{Ca})/M_{Al}$ was obtained, indicating the existence of N-A-S-H and C-(A)-S-H gels in the matrix [55]. The gels that covered on the surface of CG and BFS particles improved the compactness of hardened paste and thereby yielded the high compressive strength (Section 3.1). Whereas the incorporation of LZT had a negative effect on the compactness of microstructure. For instance, more mineral particles (covered with gels) and micro-cracks were observed with increasing LZT content. This could be attributable to the reduction of formed hydration products due to the low reactivity of LZT, thereby affecting the porosity, which could be supported by the observations of MIP. Therefore, the addition of LZT decreased the homogeneity of the pastes, as well as the compressive strength of specimens. Additionally, the presence of Zn-peak in CBL 50 and CBL 70 samples indicated that toxic metals were physically encapsulated. However, due to the lower content, other toxic metals peaks were not observed except Zn-peak in EDS spectra.

4. Conclusion

Experiment was conducted to evaluate the solidification efficiency of CG-BFS based composite geopolymer on a hazardous material i.e. LZT. The experiment has two steps i.e. optimization of composite geopolymer strength and solidification of LZT. The main conclusions were drawn as follows:

(1) Optimization of the synthesis conditions of CG-BFS based composite geopolymer was carried out by using RSM. RSM results showed that the optimal waterglass module was 1.06, alkaline content was 13.81% and the optimal curing temperature was 30 °C. Under the optimum conditions, the maximum compressive strength of 91.13 MPa was obtained. The formation of C-S-H, C-A-S-H and N-A-S-H gels improved the strength of composite geopolymer.
(2) The composite geopolymer could solidify LZT effectively and reduce its leaching toxicity. The compressive strength of solidified bodies with addition of 70% LZT fell to 21.68 MPa. The products could have the potential to substitute building materials. Additionally, the potential applications were supported by the leaching results because the leaching concentrations regarding Zn^{2+}, Pb^{2+} and Cd^{2+} did not surpass the corresponding standard limits.
(3) The mechanism regarding solidification/stabilisation was investigated with the help of chemical speciation analysis, XRD, MIP and SEM-EDS. Through XRD, it was clear that geopolymerisation reaction involved dissolution and reorganization procedure. Additionally, the formations of amorphous gels and new crystalline phase containing Zn^{2+} were observed, while Pb^{2+} and Cd^{2+} might become part of amorphous phases. The MIP and SEM results confirmed that the compact structure of geopolymer was formed after alkaline activation. These phenomena supported the physical encapsulation of LZT. While, the leaching characteristics and chemical speciation migrations manifested that these heavy metals in LZT were solidified/stabilised not only by physical means but also by chemical ways.

CRediT authorship contribution statement

Shujie Zhao: Investigation, Methodology, Formal analysis, Writing - original draft. **Ming Xia:** Software, Writing - review & editing. **Lin Yu:** Methodology, Software. **Xiao Huang:** Writing - review & editing, Validation. **Binquan Jiao:** Supervision, Conceptualization, Validation. **Dongwei Li:** Supervision, Conceptualization, Resources.

Declaration of Competing Interest

The authors declare that they have no known competing financial interests or personal relationships that could have appeared to influence the work reported in this paper.

Acknowledgement

This research did not receive any specific grant from funding agencies in the public, commercial, or not-for-profit sectors.

References

[1] National Bureau of Statistics of China, China Statistical Yearbook 2018, China Statistical Press, Beijing, 2018.
[2] J. Deng, B. Li, Y. Xiao, L. Ma, C.P. Wang, L.W. Bin, C.M. Shu, Combustion properties of coal gangue using thermogravimetry-Fourier transform infrared spectroscopy, Appl. Therm. Eng. 116 (2017) 244–252.
[3] M.X. Zhao, G.P. Zhang, K.W. Htet, M. Kwon, C.Y. Liu, Y. Xu, M.J. Tao, Freeze-thaw durability of red mud slurry-class F fly ash-based geopolymer: effect of curing conditions, Constr. Build. Mater. 215 (2019) 381–390.
[4] X.L. Guo, H.S. Shi, W.A. Dick, Compressive strength and microstructural characteristics of class C fly ash geopolymer, Cem. Concr. Comp. 32 (2) (2010) 142–147.

[5] M. Zhang, M.X. Zhao, G.P. Zhang, D. Mann, K. Lumsden, M.J. Tao, Durability of red mud-fly ash based geopolymer and leaching behavior of heavy metals in sulfuric acid solutions and deionized water, Constr. Build. Mater. 124 (2016) 373–382.
[6] B.C. McLellan, R.P. Williams, J. Lay, A. van Riessen, G.D. Corder, Costs and carbon emissions for geopolymer pastes in comparison to ordinary portland cement, J. Clean. Prod. 19 (9–10) (2011) 1080–1090.
[7] Z.H. Xu, Z. Jiang, D.D. Wu, X. Peng, Y.H. Xu, N. Li, Y.J. Qi, P. Li, Immobilization of strontium-loaded zeolite A by metakaolin based-geopolymer, Ceram. Int. 43 (5) (2017) 4434–4439.
[8] M.C.G. Juenger, F. Winnefeld, J.L. Provis, J.H. Ideker, Advances in alternative cementitious binders, Cem. Concr. Res. 41 (12) (2011) 1232–1243.
[9] F. Muhammad, M. Xia, S. Li, X. Yu, Y.H. Mao, F. Muhammad, X. Huang, B.Q. Jiao, L. Yu, D.W. Li, The reduction of chromite ore processing residues by green tea synthesized nano zerovalent iron and its solidification/stabilization in composite geopolymer, J. Clean. Prod. 234 (2019) 381–391.
[10] S.K. Nath, S. Kumar, Influence of iron making slags on strength and microstructure of fly ash geopolymer, Constr. Build. Mater. 38 (2013) 924–930.
[11] S.K. Nath, Fly ash and zinc slag blended geopolymer: immobilization of hazardous materials and development of paving blocks, J. Hazard. Mater. 387 (2020).
[12] A. Mehta, R. Siddique, T. Ozbakkaloglu, F.U.A. Shaikh, R. Belarbi, Fly ash and ground granulated blast furnace slag-based alkali-activated concrete: mechanical, transport and microstructural properties, Constr. Build. Mater. 257 (2020).
[13] F.A. Ababneh, A.I. Alakhras, M. Heikal, S.M. Ibrahim, Stabilization of lead bearing sludge by utilization in fly ash-slag based geopolymer, Constr. Build. Mater. 227 (2019).
[14] S. Celikten, M. Saridemir, I.O. Deneme, Mechanical and microstructural properties of alkali-activated slag and slag plus fly ash mortars exposed to high temperature, Constr. Build. Mater. 217 (2019) 50–61.
[15] I. Ismail, S.A. Bernal, J.L. Provis, R.S. Nicolas, S. Hamdan, J.S.J. van Deventer, Modification of phase evolution in alkali-activated blast furnace slag by the incorporation of fly ash, Cem. Concr. Comp. 45 (2014) 125–135.
[16] X.M. Liu, N. Zhang, Y. Yao, H.H. Sun, H. Feng, Micro-structural characterization of the hydration products of bauxite-calcination-method red mud-coal gangue based cementitious materials, J. Hazard. Mater. 262 (2013) 428–438.
[17] N. Zhang, X.M. Liu, H.H. Sun, L.T. Li, Pozzolanic behaviour of compound-activated red mud-coal gangue mixture, Cem. Concr. Res. 41 (3) (2011) 270–278.
[18] J.J. Geng, M. Zhou, Y.X. Li, Y.C. Chen, Y. Han, S. Wan, X. Zhou, H.B. Hou, Comparison of red mud and coal gangue blended geopolymers synthesized through thermal activation and mechanical grinding preactivation, Constr. Build. Mater. 153 (2017) 185–192.
[19] F. Slaty, H. Khoury, J. Wastiels, H. Rahier, Characterization of alkali activated kaolinitic clay, Appl. Clay Sci. 75–76 (2013) 120–125.
[20] A.D. Hounsi, G.L. Lecomte-Nana, G. Djeteli, P. Blanchart, Kaolin-based geopolymers: Effect of mechanical activation and curing process, Constr. Build. Mater. 42 (2013) 105–113.
[21] A.D. Hounsi, G. Lecomte-Nana, G. Djeteli, P. Blanchart, D. Alowanou, P. Kpelou, K. Napo, G. Tchangbedji, M. Praisler, How does Na, K alkali metal concentration change the early age structural characteristic of kaolin-based geopolymers, Ceram. Int. 40 (7) (2014) 8953–8962.
[22] R.A.A.B. Santa, C. Soares, H.G. Riella, Geopolymers with a high percentage of bottom ash for solidification/immobilization of different toxic metals, J. Hazard. Mater. 318 (2016) 145–153.
[23] Z.H. Ji, Y.S. Pei, Geopolymers produced from drinking water treatment residue and bottom ash for the immobilization of heavy metals, Chemosphere 225 (2019) 579–587.
[24] L. Wang, D.W. Cho, D.C.W. Tsang, X.D. Cao, D.Y. Hou, Z.T. Shen, D.S. Alessi, Y.S. Ok, C.S. Poon, Green remediation of As and Pb contaminated soil using cement-free clay-based stabilization/solidification, Environ. Int. 126 (2019) 336–345.
[25] F. Muhammad, X. Huang, S. Li, M. Xia, M.L. Zhang, Q. Liu, M.A.S. Hassan, B.Q. Jiao, L. Yu, D.W. Li, Strength evaluation by using polycarboxylate superplasticizer and solidification efficiency of Cr6+, Pb2+ and Cd2+ in composite based geopolymer, J. Clean. Prod. 188 (2018) 807–815.
[26] N. Ye, Y. Chen, J.K. Yang, S. Liang, Y. Hu, B. Xiao, Q.F. Huang, Y.F. Shi, J.P. Hu, X. Wu, Co-disposal of MSWI fly ash and Bayer red mud using an one-part geopolymeric system, J. Hazard. Mater. 318 (2016) 70–78.
[27] Y.C. Chen, X. Zhou, S. Wan, R. Zheng, J. Tong, H.B. Hou, T. Wang, Synthesis and characterization of geopolymer composites based on gasification coal fly ash and steel slag, Constr. Build. Mater. 211 (2019) 646–658.
[28] B.I. Ei-Eswed, O.M. Aldagag, F.I. Khalili, Efficiency and mechanism of stabilization/solidification of Pb(II), Cd(II), Cu(II), Th(IV) and U(VI) in metakaolin based geopolymers, Appl. Clay Sci. 140 (2017) 148–156.
[29] X. Huang, T. Huang, S. Li, F. Muhammad, G.J. Xu, Z.Q. Zhao, L. Yu, Y.J. Yan, D.W. Li, B. Jiao, Immobilization of chromite ore processing residue with alkali-activated blast furnace slag-based geopolymer, Ceram. Int. 42 (8) (2016) 9538–9549.
[30] Y. Cui, D.M. Wang, Y.R. Wang, R. Sun, Y.F. Rui, Effects of the n(H2O: Na2Oeq) ratio on the geopolymerization process and microstructures of fly ash-based geopolymers, J. Non-Cryst. Solids 511 (2019) 19–28.
[31] K. Komnitsas, D. Zaharaki, A. Vlachou, G. Bartzas, M. Galetakis, Effect of synthesis parameters on the quality of construction and demolition wastes (CDW) geopolymers, Adv. Powder Technol. 26 (2) (2015) 368–376.
[32] F.G.M. Aredes, T.M.B. Campos, J.P.B. Machado, K.K. Sakane, G.P. Thim, D.D. Brunelli, Effect of cure temperature on the formation of metakaolinite-based geopolymer, Ceram. Int. 41 (6) (2015) 7302–7311.
[33] USEPA, Toxicity Characteristic Leaching Procedure (Method 1311); 1992.
[34] CN-GB, Identification Standards for Hazardous Wastes-identification for Extraction Toxicity (GB5085.3-2007); 2007.
[35] A. Tessier, P.G.C. Campbell, M. Bisson, Sequential extraction procedure for the speciation of particulate trace-metals, Anal. Chem. 51 (7) (1979) 844–851.
[36] M. Khajelakzay, S.R. Bakhshi, Optimization of spark plasma sintering parameters of Si3N4-SiC composite using response surface methodology (RSM), Ceram. Int. 43 (9) (2017) 6815–6821.
[37] M. Carabajal, C.M. Teglia, S. Cerutti, M.J. Culzoni, H.C. Goicoechea, Applications of liquid-phase microextraction procedures to complex samples assisted by response surface methodology for optimization, Microchem. J. 152 (2020) 104436.
[38] V. Kumar, H. Singh, Regression analysis of surface roughness and micro-structural study in rotary ultrasonic drilling of BK7, Ceram. Int. 44 (14) (2018) 16819–16827.
[39] M. Ghanbari, A.M. Hadian, A.A. Nourbakhsh, K.J.D. MacKenzie, Modeling and optimization of compressive strength and bulk density of metakaolin-based geopolymer using central composite design: A numerical and experimental study, Ceram. Int. 43 (1) (2017) 324–335.
[40] X.Y. Zhuang, L. Chen, S. Komarneni, C.H. Zhou, D.S. Tong, H.M. Yang, W.H. Yu, H. Wang, Fly ash-based geopolymer: clean production, properties and applications, J Clean Prod 125 (2016) 253–267.
[41] D. Nasr, A.H. Pakshir, H. Ghayour, The influence of curing conditions and alkaline activator concentration on elevated temperature behavior of alkali activated slag (AAS) mortars, Constr. Build. Mater. 190 (2018) 108–119.
[42] S.J. Zhao, F. Muhammad, L. Yu, M. Xia, X. Huang, B.Q. Jiao, N. Lu, D.W. Li, Solidification/stabilization of municipal solid waste incineration fly ash using uncalcined coal gangue-based alkali-activated cementitious materials, Environ. Sci. Pollut. R. 26 (25) (2019) 25609–25620.
[43] S. Kumar, R. Kumar, S.P. Mehrotra, Influence of granulated blast furnace slag on the reaction, structure and properties of fly ash based geopolymer, J. Mater. Sci. 45 (3) (2010) 607–615.
[44] S.K. Nath, S. Kumar, Evaluation of the suitability of ground granulated silico-manganese slag in Portland slag cement, Constr. Build. Mater. 125 (2016) 127–134.
[45] S. Puligilla, P. Mondal, Role of slag in microstructural development and hardening of fly ash-slag geopolymer, Cem. Concr. Res. 43 (2013) 70–80.
[46] Z.G. Shi, C.J. Shi, S. Wan, Z.H. Ou, Effect of alkali dosage on alkali-silica reaction in sodium hydroxide activated slag mortars, Constr. Build. Mater. 143 (2017) 16–23.
[47] Q. Wan, F. Rao, S.X. Song, C.A. Leon-Patino, Y.Q. Ma, W.Z. Yin, Consolidation of mine tailings through geopolymerization at ambient temperature, J. Am. Ceram. Soc. 102 (5) (2019) 2451–2461.
[48] S. Kundu, A. Aggarwal, S. Mazumdar, K.B. Dutt, Stabilization characteristics of copper mine tailings through its utilization as a partial substitute for cement in concrete: preliminary investigations, Environ. Earth Sci. 75 (3) (2016).
[49] J.G. Zhang, J.L. Provis, D.W. Feng, J.S.J. van Deventer, Geopolymers for immobilization of Cr6+, Cd2+, and Pb2+, J. Hazard. Mater. 157 (2–3) (2008) 587–598.
[50] A. Al-Mashqbeh, S. Abuali, B. El-Eswed, F.I. Khalili, Immobilization of toxic inorganic anions (Cr2O72-, MnO4- and Fe(CN)(6)(3-)) in metakaolin based geopolymers: a preliminary study, Ceram. Int. 44 (5) (2018) 5613–5620.
[51] X. Huang, R.L. Zhuang, F. Muhammad, L. Yu, Y.C. Shiau, D.W. Li, Solidification/stabilization of chromite ore processing residue using alkali-activated composite cementitious materials, Chemosphere 168 (2017) 300–308.
[52] S. Lee, A. van Riessen, C.M. Chon, N.H. Kang, H.T. Jou, Y.J. Kim, Impact of activator type on the immobilisation of lead in fly ash-based geopolymer, J. Hazard. Mater. 305 (2016) 59–66.
[53] S. Li, X. Huang, F. Muhammad, L. Yu, M. Xia, J. Zhao, B.Q. Jiao, Y. Shiau, D.W. Li, Waste solidification/stabilization of lead-zinc slag by utilizing fly ash based geopolymers, RSC Adv. 8 (57) (2018) 32956–32965.
[54] Z.H. Zhang, L.F. Li, X. Ma, H. Wang, Compositional, microstructural and mechanical properties of ambient condition cured alkali-activated cement, Constr. Build. Mater. 113 (2016) 237–245.
[55] H. Xu, W.L. Gong, L. Syltebo, K. Izzo, W. Lutze, I.L. Pegg, Effect of blast furnace slag grades on fly ash based geopolymer waste forms, Fuel 133 (2014) 332–340.
[56] K. Gao, K.L. Lin, D. Wang, C.L. Hwang, H.S. Shiu, Y.M. Chang, T.W. Cheng, Effects SiO2/Na2O molar ratio on mechanical properties and the microstructure of nano-SiO2 metakaolin-based geopolymers, Constr. Build. Mater. 53 (2014) 503–510.
[57] Q. Dong, B. Liang, L.F. Jia, L.G. Jiang, Effect of sulfide on the long-term strength of lead-zinc tailings cemented paste backfill, Constr. Build. Mater. 200 (2019) 436–446.
[58] H.A. Abdel-Gawwad, S.A. Mohamed, M.S. Mohammed, Recycling of slag and lead-bearing sludge in the cleaner production of alkali activated cement with high performance and microbial resistivity, J. Clean. Prod. 220 (2019) 568–580.
[59] N. Koshy, K. Dondrob, L.M. Hu, Q. Wen, J.N. Meegoda, Synthesis and characterization of geopolymers derived from coal gangue, fly ash and red mud, Constr. Build. Mater. 206 (2019) 287–296.